JACS
JOURNAL OF THE AMERICAN CHEMICAL SOCIETY
Article
pubs.acs.org/JACS

Size Specifically High Activity of Ru Nanoparticles for Hydrogen Oxidation Reaction in Alkaline Electrolyte

Junya Ohyama,*[†,‡] Takuma Sato,[†] Yuta Yamamoto,[§] Shigeo Arai,[§] and Atsushi Satsuma[†,‡]

[†]Graduate School of Engineering and [§]Ecotopia Science Institute, Nagoya University, Nagoya 464-8603, Japan
[‡]Elements Strategy Initiative for Catalysts and Batteries (ESICB), Kyoto University, Katsura, Kyoto 615-8520, Japan

Supporting Information

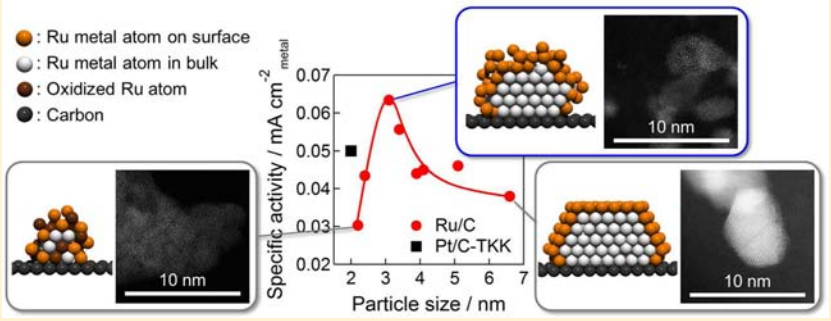

ABSTRACT: The hydrogen oxidation reaction (HOR) in alkaline electrolyte was conducted on carbon-supported Ru nanoparticles (Ru/C) of which size was controlled in the range from approximately 2 to 7 nm. The HOR activity of Ru/C normalized by the metal surface area showed volcano shaped dependence on the particle size with a maximum activity at approximately 3 nm. The HOR activity of approximately 3 nm Ru/C was higher than commercially available Pt nanoparticles (ca. 2 nm) supported on carbon. The structural analysis of Ru/C using Cs-corrected scanning transmission electron microscopy with atomic resolution revealed the unique structural change of Ru/C different from Pt/C: Ru nanoparticle structure changed from amorphous-like structure below 3 nm to metal nanocrystallite with roughened surface at approximately 3 nm and then to that with well-defined facets above 3 nm, although Pt/C kept well-defined facets even at approximately 2 nm. It is proposed that the generation of unique structure observed on approximately 3 nm Ru nanoparticles, that is, long bridged coordinatively unsaturated Ru metal surface atoms on its nanocrystallite, is a key to achieve high HOR activity.

INTRODUCTION

Polymer electrolyte fuel cells are promising power sources due to their high energy efficiency and environmental compatibility; however, their high cost due to a Pt-based catalyst has hampered their large-scale commercialization. Fine control of the nanocatalyst structure is one of the key strategies to improve the catalytic performance and reduce Pt usage.[1−5] Hydrogen oxidation reaction (HOR) on a fuel cell anode catalyst is a structure sensitive reaction as represented by the different HOR activity between metal single-crystal surfaces.[6−9] Recent study of the HOR on Pt nanoparticles with cuboctahedral shape demonstrated that their size has an influence on the catalytic activity due to the change in fraction of facet, edge, and corner.[2] The oxygen reduction reaction (ORR) on a cathode catalyst also varies with the metal particle size.[4,10−12] Besides fuel cell catalysts, size control of metal nanoparticle produces unique catalytic properties, and well-designed nanosized non-Pt metal catalysts sometimes show higher performance than a Pt catalyst.[13,14] These beneficial and attractive effects of structural control inspired us to develop a non-Pt anode catalyst having higher or comparable catalytic activity to Pt by fine-tuning of the catalyst structure in nanoscale. On the other hand, recent progress in electron microscopy allows us to observe catalyst structure in the atomic level. Such microscopic analysis has revealed that the atomic level structure significantly affects the catalytic activity.[10,15,16] Thus, the atomic level study is required not only to improve catalytic activity but also to understand the fundamentals of the structural effect.

Anion-exchange membrane fuel cells (AEMFCs) have attracted considerable attention due to their applicability of non-Pt metal catalysts in the less corrosive environment than proton-exchange membrane fuel cells (PEMFCs).[17,18] Non-Pt metal catalysts have been widely investigated for the cathode electrocatalysts of AEMFCs. However, for the anode electrodes, there are a few studies about non-Pt catalysts.[19,20] Very recently, we applied various metal particles supported on carbon to the anode electrode of an AEMFC single cell, and Ru nanoparticles supported on carbon (Ru/C) exhibited high performance comparable to a commercially available Pt/C catalyst (Tanaka Kikinzoku Kogyo, particle size 2 nm, 50 wt %, denoted as Pt/C-TKK).[21]

Received: March 1, 2013
Published: April 23, 2013

dx.doi.org/10.1021/ja4021638 | J. Am. Chem. Soc. 2013, 135, 8016−8021

Size, shape, and structure of the Ru nanoparticle catalyst often have a significant influence on its catalytic property. Park, Somorjai, and co-workers demonstrated that the size of Ru nanoparticles affects CO oxidation activity.[22] They identified the highly active Ru species and its size-dependent stability, which is the origin of the size effect on CO oxidation.[23] Zhang, Yan, and co-workers finely controlled the morphology of Ru nanocrystallite and showed the morphology-dependent catalytic activity for CO selective methanation as well as surface enhanced Raman spectra (SERS) property.[24] The size effect on the catalytic activity of Ru nanoparticles has been reported on CO and CO_2 methanation,[25−27] NH_3 synthesis,[28] Fischer−Tropsch synthesis,[29,30] and oxidation of acetic acid.[31] Very recently, Kitagawa et al. reported high CO oxidation activity of newly synthesized Ru nanoparticles having face-centered cubic (fcc) structure and its unique size-dependent catalytic performance.[32] These studies provide rational design of the Ru nanoparticle catalyst for development of the performance and practical application.

In the present study, we demonstrate the unique size-dependent HOR activity of Ru nanoparticles. Although it has been reported that HOR activity of a Ru catalyst is at least 2−3 orders of magnitude lower than that of a Pt catalyst in acidic electrolyte due to the high oxophilicity of Ru, our study presents that the well-controlled Ru/C exhibits higher mass and specific activity than Pt/C-TKK in alkaline electrolyte. Furthermore, very interestingly, the size effect of Ru nanoparticles was quite different from that of Pt, and Ru nanoparticles showed size-specific high activity due to the unique structural change with the particle size.

EXPERIMENTAL SECTION

Size Controlled Synthesis of Ru/C. The chemical reagents used in this study were purchased from Kishida Chemical Co., Ltd. unless described otherwise. Ru/C catalyst (50 wt % Ru loading) was prepared by liquid phase reduction of an isopropanol and aqueous solution of $RuCl_3$ using $NaBH_4$ in the presence of Vulcan XC-72R. To 300 mL of $RuCl_3$ aqueous solution (3.3 mmol L^{-1}) containing 15 mL of isopropanol (for well dispersion of carbon) was added NaOH aqueous solution (0.1 mol L^{-1}) to control the pH = 7, followed by addition of 100 mg of Vulcan XC-72R. The temperature of suspension was controlled in a water or ice bath at 0, 10, 25, and 35 °C. The Ru precursor was reduced with 100 mL of $NaBH_4$ aqueous solution (10 mmol) whose temperature was also controlled. After stirring for 0.5 h, the suspension was filtered, and the residue was washed with 200 mL of water. The resulting black powder was dried at 353 K overnight. The Ru/C prepared at 25 °C was treated at 100, 200, 300, and 400 °C under H_2. As references, Pt/C (46 wt %) purchased from Tanaka Kikinzoku Kogyo (Pt/C-TKK) was treated at 100, 500, 650, 700, and 750 °C under N_2 to control the Pt particle size.

Electrochemical Measurement. Electrochemical measurements were conducted using the rotating disk electrode (RDE) setup with a potentiostat (HZ-5000 (HAG-3001), Hokuto Denko Corp.). Catalyst ink was prepared by ultrasonic mixing of a suspension of 19.6 mg of catalyst in a mixed solution of 2.5 mL of 1-hexanol. The catalyst ink was dropped on the glassy carbon substrate of the RDE electrode (HR2-D1-GC-5, 5 mm in diameter, 0.196 cm^2) to be 10 μg_{Ru} cm_{disk}^{-2} (Figure S1, Supporting Information). After the ink was dried on the substrate, 5 μL of a diluted ionomer solution (0.05 wt % in 1-propanol prepared from AS-4 solution (5 wt % in 1-propanol, Tokuyama Corp.)) was dropped on the disk. The HOR was carried out in an H_2-purged 0.1 M NaOH aqueous solution using a three-electrode cell with a Pt wire as the counter electrode and a RHE electrode (Miclab Co., Ltd.) as the reference electrode. The NaOH solution was bubbled with N_2 (100 mL min^{-1}) by purging for 0.5 h and then with H_2 (100 mL min^{-1}) for at least 0.5 h. The catalysts were pretreated in the electrolyte by repetition of linear sweep from −0.05 to 0.9 V at 10 mV s^{-1}. After the voltammogram did not change, the polarization curve for the HOR was recorded by sweeping the potential from 0.2 to 0.9 V versus RHE (scan rate: 10 mV s^{-1}; rotation rate: 400, 900, 1600, and 2500 rpm; temperature: 25 °C). In the same manner, the HOR in H_2SO_4 aqueous solution was also obtained using Nafion solution (0.05 wt %) as ionmer.

Cyclic voltammograms (CVs) for the Ru/C were obtained in a N_2-purged 0.1 M NaOH solution at 25 °C from 0.05 to 0.9 V versus RHE at 50 mV s^{-1}, after the pretreatment by cyclic voltammetry from 0.1 to 1.0 V versus RHE at 500 mV s^{-1} (100 cycles).

Cu_{upd} stripping voltammetry (0.3−0.9 V vs RHE, 10 mV s^{-1}) was performed in a N_2-purged 0.1 M H_2SO_4 solution containing 2 mM $CuSO_4$ at 25 °C after Cu deposition at 0.3 V versus RHE for 100 s. Before the voltammetry, the catalysts were pretreated by CV (0.1−1 V vs RHE, 500 mV s^{-1}, 100 cycles) in 0.1 M H_2SO_4 solution without $CuSO_4$. For Ru/C, further CV pretreatment (0−0.01 V vs RHE, 0.1 mV s^{-1}) was carried out until the voltammogram did not change. The voltammogram on each catalyst in 0.1 M H_2SO_4 solution without $CuSO_4$ (0.3−0.9 V vs RHE, 10 mV s^{-1}) was applied as the background for the corresponding Cu_{upd} stripping voltammogram.

Transmission Electron Microscopy and Cs-Corrected Scanning Transmission Electron Microscopy Observation. The metal particle size was analyzed by observation using a HITACHI H-800 transmission electron microscope operated at 200 kV. The fine structure of the catalyst was observed using a JEOL-200 kV Cs-corrected S/TEM with atomic resolution.

RESULTS AND DISCUSSION

The Ru/C catalysts prepared in various conditions were observed by transmission electron microscopy (TEM) to evaluate the particle size (Figure S2, Supporting Information). As listed in Table 1, approximately 2−7 nm Ru nanoparticles supported on carbon were obtained. X-ray diffraction (XRD) analysis revealed that the Ru/C catalysts greater than 3 nm have hexagonal close-packed (hcp) structure and the Ru/C less than 3 nm have amorphous-like structure (Figure S3, Supporting Information). Figure 1a shows the polarization curves obtained on the Ru/C catalysts in 0.1 M NaOH aqueous solution saturated with H_2 at 2500 rpm. The HOR current for all of the samples increased with positive-going sweeps up to around 0.2 V and then decreased. Similar features were also observed in the CVs shown in Figure 1b. The CV peaks around 0.15 V are derived from desorption (oxidation) of underpotentially deposited hydrogen (H_{upd}) and the Ru surface oxidation.[6,8,33] Because the oxygenated species on Ru inhibits H_2 adsorption, the HOR current shown in Figure 1a decreased

Table 1. Diameter, ECSA, CSA, and Ratio of ECSA/CSA for Ru/C Prepared or Treated at Various Temperatures

temp (°C)	diameter[c] (nm)	ECSA[d] (m^2 g^{-1})	CSA[e] (m^2 g^{-1})	ECSA/CSA
0[a]	2.2 ± 0.8	100	219	0.46
10[a]	2.4 ± 0.8	107	201	0.53
25[a]	3.1 ± 1.3	131	156	0.86
35[a]	3.4 ± 1.3	126	142	0.89
100[b]	3.9 ± 1.8	112	124	0.90
200[b]	4.1 ± 1.7	110	118	0.93
300[b]	5.1 ± 2.1	85	95	0.90
400[b]	6.6 ± 2.8	65	73	0.89

[a]For the preparation by a liquid phase reduction. [b]For the heat treatment of Ru/C prepared at 25 °C. [c]Evaluated by TEM observation. [d]Determined by Cu_{upd} stripping voltammetry. [e]Calculated from the diameter assuming spherical Ru particle.

dx.doi.org/10.1021/ja4021638 | J. Am. Chem. Soc. 2013, 135, 8016−8021

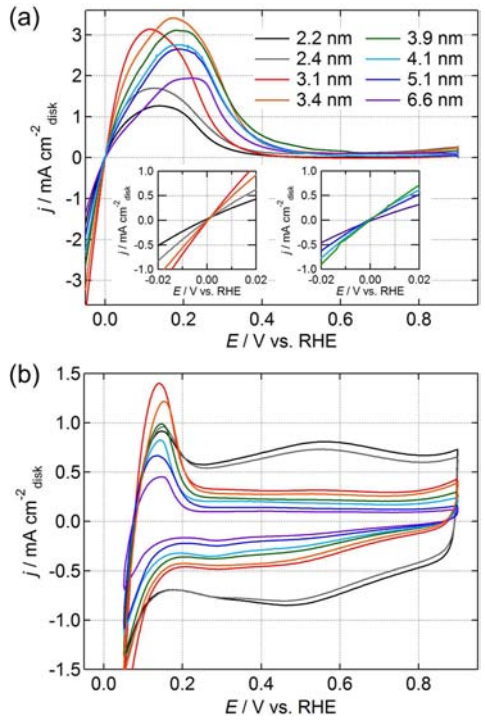

Figure 1. (a) Polarization curves obtained on Ru/C catalysts in 0.1 M NaOH aqueous solution saturated with H_2. Sweep rate: 10 mV s^{-1}; rotation rate: 2500 rpm; temperature: 25 °C. (b) CVs of Ru/C catalysts in 0.1 M NaOH aqueous solution saturated with N_2. Sweep rate: 50 mV s^{-1}; temperature: 25 °C.

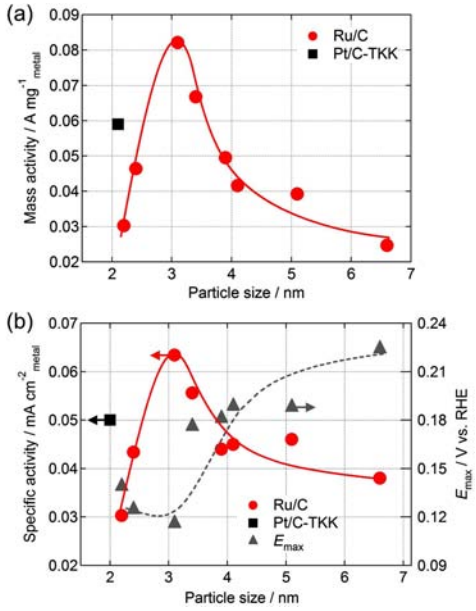

Figure 2. Plots of (a) the mass activity and (b) the specific activity and the potential at maximum HOR current (E_{max}) for the Ru/C against the mean particle size, together with the mass and specific activities of Pt/C-TKK as a reference.

above 0.2 V. The surface oxidation also caused the absence of a clearly defined Tafel region where the exchange current can be determined by extrapolating the Tafel lines (Figure S4, Supporting Information). Therefore, we evaluated the exchange current (i_0) from the linear-current potential region from −0.02 to 0.02 V versus RHE (the inserts in Figure 1a) using the approximate Butler−Volmer equation $i = i_0(n\eta F/RT)$, where n is the exchange electron number, η is the applied overpotential ($|\eta| \leq 0.02$ V), and R and F have conventional meanings.[34] The n values for the HOR on all of the Ru/C were determined to be two from a Koutecky−Levich plot analysis (Figure S5, Supporting Information). By using the n value, the i_0 value was calculated from the slope of the linear-current potential region and normalized by Ru weight on a disk electrode to evaluate the mass activity (MA), that is, the efficiency of metal utilization. Figure 2a shows the mass activity dependence on the Ru particle size. The mass activity drastically increased with an increase in the size from 2.2 to 3.1 nm and then decreased. Thus, the 3.1 nm Ru nanoparticles represented the highest mass activity. For comparison, we also evaluated the HOR activity of Pt/C-TKK. As a result, the approximately 3 nm Ru/C catalysts showed higher mass activity than Pt/C-TKK. This result is well consistent with our previous AEMFC single cell test with a Ru/C anode catalyst showing higher power density than that with Pt/C-TKK.[21]

If there is no structural effect on the HOR, the mass activity decreases with an increase in the particle size because large particles have small surface area per weight. However, the Ru/C exhibited the volcano-type dependent mass activity on the particle size, indicating that the catalyst per each atom varies with the particle size. Thus, we investigated the catalytic activity of each Ru atom of the Ru/C catalysts by normalizing the i_0 with the electrochemically accessible surface area (ECSA) to obtain the specific activity. The ECSA was determined by a Cu underpotential deposition (Cu_{upd}) stripping voltammetry (Figure S6, Supporting Information) as listed in Table 1. The specific activity was plotted against the Ru nanoparticle size in Figure 2b. The specific activity showed volcano-shaped size dependence, and the maximum value was obtained at 3.1 nm. Thus, the 3.1 nm Ru/C has the most highly active species for the HOR. Furthermore, the approximately 3 nm Ru/C showed higher specific activity than as-purchased Pt/C-TKK (2.1 nm). Interestingly, but unfortunately, in acidic electrolyte, the HOR activity of the 3.1 nm Ru/C was much lower than that of Pt/C-TKK, which is consistent with the previous study by Gasteiger et al. that Ru showed much lower activity than Pt as described above.[6] Moreover, the HOR activity on Ru/C in acidic electrolyte was also lower than that in alkaline electrolyte (Figures S7 and S8, Supporting Information). On the contrary, it has been reported that the abundance of OH^- in alkaline electrolyte decreases the HOR activity due to more site blocking by adsorbed OH species and/or stronger binding energy of metal−H than that in acidic electrolyte.[34,35] Although at this moment we cannot address the role of OH^- in the HOR on Ru/C, OH^- might act as the promoter of the HOR on the Ru/C. The effect of OH^- will be the subject of future study.

Figure 2b also shows the potential at maximum HOR current (E_{max}) plotted against the Ru particle size. The E_{max} did not significantly change within 3.1 nm but increased above that size. This result indicates that the Ru/C with less than or equal to 3.1 nm has high oxophilicity to form surface oxygenated species at lower potential than those having larger particle size. The high oxophilicity usually reduces the HOR activity due to the susceptibility to the formation of surface oxygenated species. However, the 3.1 nm Ru/C showed the highest HOR activity. Adzic and co-workers reported the higher HOR reaction kinetics on Ru(10-10) than Ru(0001) in spite of the faster oxidation of Ru(10-10).[8] They proposed that the unsaturated atoms of Ru(10-10) can adsorb H_2 even in the presence of

dx.doi.org/10.1021/ja4021638 | J. Am. Chem. Soc. 2013, 135, 8016−8021

surface oxygenated species in the ridges of Ru(10-10), although such species on a flat Ru(0001) inhibit H_2 adsorption. No inhibition of the HOR by the surface oxygenated species was also seen on Pt(110), which has more coordinatively unsaturated Pt atoms and higher HOR activity than Pt(111) and Pt(100), despite the larger coverage with the oxygenated species on Pt(110) surface.[36] Therefore, it is proposed that the 3.1 nm Ru/C has coordinatively unsaturated atoms to conduct the HOR in spite of its susceptibility to the surface oxidation. Actually, the 3.1 nm Ru/C showed the similar polarization curve for the HOR to Ru(10-10).[8]

To inspect the structure of Ru nanoparticles, we observed Ru/C catalysts by using Cs-corrected scanning transmission electron microscopy (STEM). Figure 3 shows the typical high angle annular dark field (HAADF) STEM images of Ru/C having 2.2, 3.1, and 6.6 nm. Large fraction of the 2.2 nm Ru nanoparticles displayed amorphous-like structure. Such Ru nanoparticles would keep Ru oxide species, causing low HOR activity as described below. The Ru species with amorphous-like structure were also observed on the 3.1 nm Ru/C but together with lattice fringes due to Ru metal crystal. This result suggests that the 3.1 nm Ru/C has Ru metal nanocrystallite covered with amorphous-like layers, that is, Ru nanoparticles with roughened surface, as illustrated in Figure 3d. On the other hand, the 6.6 nm Ru/C exhibited Ru nanoparticles with clear lattice fringes and facets. On the basis of these results, we propose the relationship between the structure and catalytic activity as follows: Ru nanoparticles with roughened surface are more active to the HOR than those with well-defined facet, although too large fraction of coordinatively unsaturated Ru atoms decreases the activity because of their high susceptibility to oxidation.

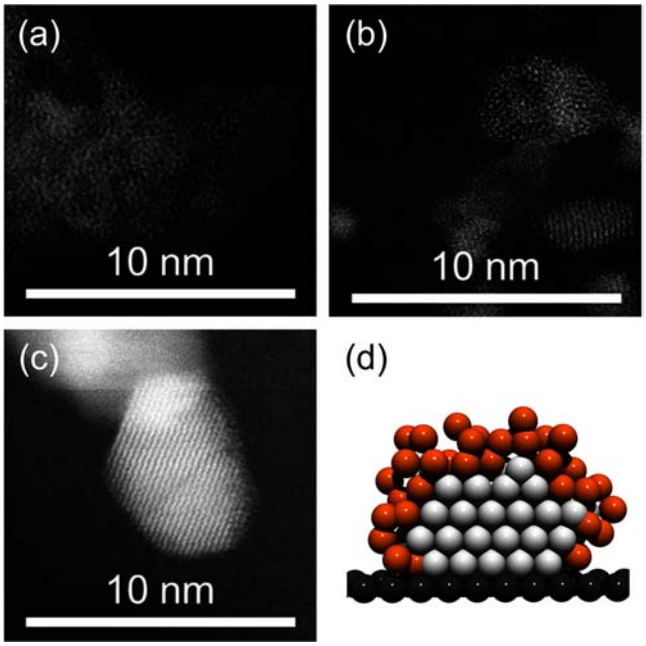

Figure 3. HAADF STEM images of Ru/C with (a) 2.2, (b) 3.1, and (c) 6.6 nm. (d) Illustration of the structure of the 3.1 nm Ru/C. Yellow: amorphous-like surface Ru atoms; gray: Ru atoms in its nanocrystallite; black: carbon support.

For investigation of the size-dependent oxophilicity, we calculated the ratio of ECSA to the chemical surface area (CSA) that is determined from the Ru particle size as listed in Table 1. The Ru/C with less than 3 nm Ru nanoparticles represented an obviously low ECSA/CSA ratio (ca. 50%) compared to the other Ru catalysts. This indicates the existence of Ru oxide in the Ru/C less than 3 nm (not only on the surface but also in the bulk). In fact, the Ru/C less than 3 nm (Figure 2) presented the similar CV feature to Ru oxide reported elsewhere (cathodic peak at ca. 0.56 V, anodic peak at ca. 0.46 V) together with that of Ru metal (cathodic peak at ca. 0.15 V, anodic peak (shoulder) at ca. 0.29 V).[37] Furthermore, the X-ray photoelectron (XP) and X-ray absorption fine structure (XAFS) spectroscopy analyses indicated that as-prepared Ru/C less than 3 nm is in a more oxidized state than those having larger Ru nanoparticles (Figures S9−11, Supporting Information). Thus, the Ru/C less than 3 nm are unstable in the metal state and not completely reduced to metal due to the significantly large fraction of coordinatively unsaturated Ru atoms as indicated by STEM observation and XRD analysis (Figure S3, Supporting Information). The oxidized surface of Ru nanoparticles would inhibit the dissociative adsorption of H_2 (Tafel step), causing the decrease in the HOR activity. This consideration agrees with the previous study on the HOR on Pt particles by Bayati et al. that the oxidation of unsaturated Pt atoms results in the decrease of activity to the electrochemical oxidation of methanol.[38] On the other hand, when the Ru particles grow above 3 nm, the ECSA/CSA ratio did not depend on the size and was approximately 90%. The data suggest that all of Ru nanoparticles with greater than 3 nm are composed of Ru metal. However, above 3 nm, the HOR activity decreased with an increase in the size (Figure 2b). The STEM observation revealed the increase in the size of Ru nanoparticles greater than 3 nm forms a flat surface such as Ru(0001) that has low HOR activity than a surface having coordinatively unsaturated atoms such as Ru(10-10). Therefore, we conclude that the approximately 3 nm Ru/C has coordinatively unsaturated "metal" atoms exhibiting high activity to the HOR.

For comparison, we also prepared Pt/C catalysts having various sizes by the heat treatment of Pt/C-TKK from 100 to 750 °C (Figure S12, Supporting Information). The mass and specific activities of the Pt/C catalysts for the HOR were determined in the same way as the Ru/C (Figures S13−15, Supporting Information) and are shown in Figure 4. The mass activity of Pt/C represented the maximum value at 3−3.5 nm, agreeing the previous report on the Pt particle size effect for the HOR in acidic electrolyte.[2] For practical interesting, it is noteworthy that the mass activity of Ru/C with approximately

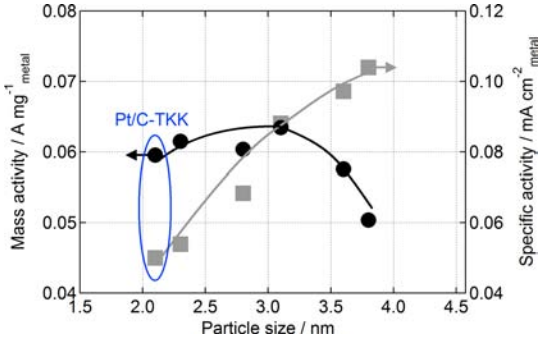

Figure 4. Plots of the mass and specific activities of the Pt/C against the mean particle size.

dx.doi.org/10.1021/ja4021638 | J. Am. Chem. Soc. 2013, 135, 8016−8021

3 nm diameter was higher than the maximum mass activity of Pt/C in alkaline electrolyte. On the other hand, the specific activity increased with an increase in the particles size, which is also consistent with the previous report on the Pt-size-dependent specific activity in acidic electrolyte.[2] The specific activity of Pt/C will reach to almost plateau value as the particle size increases, because the ratio of Pt atoms on facet to the total atoms on the surface increases with an increase in the particle size and then reaches to almost plateau.

Very recently, Chen et al. studied the Pt size effect on the HOR in acidic electrolyte and proposed that the decrease in the HOR activity with the decrease in the size is due to the increase in the fraction of edge atoms that are less active than those on the facets. The edge atom rows of Pt particles with cuboctahedral shape have a similar structure to the Pt(110) surface, and the facets have Pt(100) and (111) surfaces.[2] Thus, the Pt(110) row on the particle edges has lower HOR activity than Pt(100) and (111) facets. On the other hand, previous studies by Markovic and co-workers have shown that the extended Pt(110) surface has higher HOR activity than Pt(111) and (100) surfaces, since the Pt(110) dissociatively adsorbs H_2 with low activation energy and remains the H_2 adsorption ability even in the presence of the surface oxygenated species.[9,36] The difference in the HOR activity between the row and the extended surface Pt(110) can be explained by the variation of the distribution of hydrogen adsorption sites with surface geometry, that is, the edge row for the Pt particle or the long bridged row for the extended surface. In this study, we actually observed Pt/C-TKK and that treated at 750 °C by using CSTEM as shown in Figure 5. The HAADF

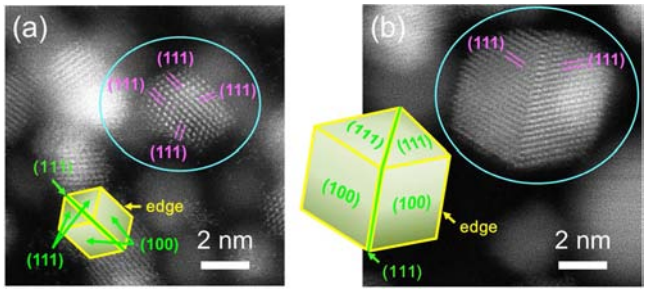

Figure 5. HAADF STEM images of (a) Pt/C-TKK and (b) that were treated at 750 °C. The estimated morphologies and exposed surfaces of particles indicated by the circle were illustrated on the images.[39]

STEM image of Pt/C-TKK exhibited Pt nanocrystallites with (111) twin boundary (Figure 5a) as well as single crystallites (Figure S16a, Supporting Information).[39] They exhibited well-defined facets. The heat-treated Pt nanoparticles also exhibited (111) twin (Figure 5b) and single crystallites (Figure S16b, Supporting Information), which have larger facet than Pt/C-TKK. The exposed surfaces are assignable to Pt(111) and Pt(100) as illustrated in Figure 5. Thus, we concluded that the facets of the Pt nanoparticle are more active for the HOR than the edge in alkaline electrolyte as they are in acidic electrolyte.

Note that the size effect for the specific activity was particularly different between Ru and Pt. This will be due to their different variations of particle morphology with size. The increase in the size of Ru nanoparticles from approximately 2 to 3 nm enhanced the crystallinity of Ru metal but the roughened surface remained. Further growth of Ru nanoparticles generated the well-defined facets. Too high fraction of unsaturated Ru atoms without Ru metal crystallite and the well-defined facets reduced the specific activity due to the existence of Ru oxide and surface poisoning by the oxygenated species, respectively. As a result, the 3.1 nm Ru nanoparticles having roughened surface on Ru metal crystallite showed the highest HOR activity. On the other hand, the morphology of Pt nanoparticles did not vary with the size and exhibited well-defined facets even at approximately 2 nm. The small Pt nanoparticles had low specific activity due to the high fraction of the less active Pt(110) edge row; however, the extended Pt(110), that is, long bridged unsaturated atoms, are more active to the HOR than Pt(100) and Pt(111). On the basis of these results, we propose that the size specifically high activity of 3 nm Ru nanoparticles originates from the generation of long bridged unsaturated Ru metal atoms on its nanocrystallites.

■ CONCLUSION

The catalytic activity of Ru/C showed the volcano-shaped dependence on the Ru particle size, and the highest activity was obtained at approximately 3 nm. The 3 nm Ru/C achieved a higher HOR performance than commercially available Pt/C-TKK in alkaline electrolyte. The structural analysis using Cs-corrected STEM with atomic resolution suggested that the long bridged unsaturated surface atoms on Ru nanocrystallites are highly active for the HOR but too large fraction of unsaturated atoms and the growth of facets decrease the activity. Thus, our study demonstrates that the fine control of particle structure (size, crystallinity, and surface morphology) is indispensably required for non-Pt catalysts to obtain higher or comparable HOR activity to Pt catalysts.

■ ASSOCIATED CONTENT

Supporting Information

Optimization of catalyst loading on RDE, TEM images, XRD, Tafel plots, Koutecky–Levich plots, Cu_{upd} and H_{upd} stripping voltammograms, the HOR on Ru/C in an acid electrolyte, the HOR on Pt/C, XPS, XAFS, and HAADF STEM images. This material is available free of charge via the Internet at http://pubs.acs.org.

■ AUTHOR INFORMATION

Corresponding Author

ohyama@apchem.nagoya-u.ac.jp

Notes

The authors declare no competing financial interest.

■ ACKNOWLEDGMENTS

This study was supported by Grant-in-Aid from the Ministry of Education, Culture, Sports, Science and Technology, Japan (MEXT) program "Elements Strategy Initiative to Form Core Rersearch Center" (since 2012). The XAFS measurement was carried out by the approvals of the Photon Factory Program Advisory Committee (2012G763). The authors thank Prof. Tsukasa Torimoto (Nagoya University) for advice about the electrochemistry on Ru/C, Prof. Hisao Yoshida (Kyoto University) for XAFS measurement, Prof. Nobuo Tanaka (Nagoya University) for STEM analysis, and Tokuyama Co. for the supply of AS-4 ionomer solution.

■ REFERENCES

(1) Chen, A.; Holt-Hindle, P. *Chem. Rev.* **2010**, *110*, 3767.

(2) Sun, Y.; Dai, Y.; Liu, Y.; Chen, S. *Phys. Chem. Chem. Phys.* **2012**, *14*, 2278.
(3) Rao, C. V.; Viswanathan, B. *J. Phys. Chem. C* **2010**, *114*, 8661.
(4) Shao, M.; Peles, A.; Shoemaker, K. *Nano Lett.* **2011**, *11*, 3714.
(5) Takeguchi, T.; Yamanaka, T.; Asakura, K.; Muhamad, E. N.; Uosaki, K.; Ueda, W. *J. Am. Chem. Soc.* **2012**, *134*, 14508.
(6) Gasteiger, H. A.; Markovic, N. M.; Ross, P. N. *J. Phys. Chem.* **1995**, *99*, 8290.
(7) Gasteiger, H. A.; Markovic, N. M.; Ross, P. N. *J. Phys. Chem.* **1995**, *99*, 16757.
(8) Inoue, H.; Wang, J. X.; Sasaki, K.; Adzic, R. R. *J. Electroanal. Chem.* **2003**, *554*−*555*, 77.
(9) Markovic, N. M.; Sarraf, S. T.; Gasteiger, H. A.; Ross, P. N. *J. Chem. Soc., Faraday Trans.* **1996**, *92*, 3719.
(10) Wang, J. X.; Inada, H.; Wu, L.; Zhu, Y.; Choi, Y.; Liu, P.; Zhou, W.-P.; Adzic, R. R. *J. Am. Chem. Soc.* **2009**, *131*, 17298.
(11) Xiao, L.; Zhuang, L.; Liu, Y.; Lu, J.; Abruna, H. D. *J. Am. Chem. Soc.* **2008**, *131*, 602.
(12) Shao, M.; Yu, T.; Odell, J. H.; Jin, M.; Xia, Y. *Chem. Commun.* **2011**, *47*, 6566.
(13) Haruta, M. *Catal. Today* **1997**, *36*, 153.
(14) Shimizu, K.; Sugino, K.; Sawabe, K.; Satsuma, A. *Chem.—Eur. J.* **2009**, *15*, 2341.
(15) Herzing, A. A.; Kiely, C. J.; Carley, A. F.; Landon, P.; Hutchings, G. J. *Science* **2008**, *321*, 1331.
(16) Ohyama, J.; Esaki, A.; Yamamoto, Y.; Arai, S.; Satsuma, A. *RSC Adv.* **2013**, *3*, 1033.
(17) Zhang, H.; Shen, P. K. *Chem. Rev.* **2012**, *112*, 2780.
(18) Varcoe, J. R.; Slade, R. C. T. *Fuel Cells* **2005**, *5*, 187.
(19) Lu, S. F.; Pan, J.; Huang, A. B.; Zhuang, L.; Lu, J. T. *Proc. Natl. Acad. Sci. U.S.A.* **2008**, *105*, 20611.
(20) Asazawa, K.; Yamada, K.; Tanaka, H.; Oka, A.; Taniguchi, M.; Kobayashi, T. *Angew. Chem., Int. Ed.* **2007**, *46*, 8024.
(21) Ohyama, J.; Sato, T.; Satsuma, A. *J. Power Sources* **2013**, *225*, 311.
(22) Joo, S. H.; Park, J. Y.; Renzas, J. R.; Butcher, D. R.; Huang, W.; Somorjai, G. A. *Nano Lett.* **2010**, *10*, 2709.
(23) Qadir, K.; Joo, S. H.; Mun, B. S.; Butcher, D. R.; Renzas, J. R.; Aksoy, F.; Liu, Z.; Somorjai, G. A.; Park, J. Y. *Nano Lett.* **2012**, *12*, 5761.
(24) Yin, A.-X.; Liu, W.-C.; Ke, J.; Zhu, W.; Gu, J.; Zhang, Y.-W.; Yan, C.-H. *J. Am. Chem. Soc.* **2012**, *134*, 20479.
(25) Dagle, R. A.; Wang, Y.; Xia, G.-G.; Strohm, J. J.; Holladay, J.; Palo, D. R. *Appl. Catal., A* **2007**, *326*, 213.
(26) Abe, T.; Tanizawa, M.; Watanabe, K.; Taguchi, A. *Energy Environ. Sci.* **2009**, *2*, 315.
(27) Urasaki, K.; Endo, K.; Takahiro, T.; Kikuchi, R.; Kojima, T.; Satokawa, S. *Top. Catal.* **2010**, *53*, 707.
(28) Fishel, C. T.; Davis, R. J.; Garces, J. M. *J. Catal.* **1996**, *163*, 148.
(29) Kellner, C. S.; Bell, A. T. *J. Catal.* **1982**, *75*, 251.
(30) Kang, J.; Zhang, S.; Zhang, Q.; Wang, Y. *Angew. Chem., Int. Ed.* **2009**, *48*, 2565.
(31) Gallezot, P.; Chaumet, S.; Perrard, A.; Isnard, P. *J. Catal.* **1997**, *168*, 104.
(32) Kusada, K.; Kobayashi, H.; Yamamoto, T.; Matsumura, S.; Sumi, N.; Sato, K.; Nagaoka, K.; Kubota, Y.; Kitagawa, H. *J. Am. Chem. Soc.* **2013**, *135*, 5493−5496.
(33) Hadzi-Jordanov, S.; Angerstein-Kozlowska, H.; Vukovic, M.; Conway, B. E. *J. Phys. Chem.* **1977**, *81*, 2271.
(34) Schmidt, T. J.; Ross, P. N., Jr.; Markovic, N. M. *J. Electroanal. Chem.* **2002**, *524*−*525*, 252.
(35) Sheng, W.; Gasteiger, H. A.; Shao-Horn, Y. *J. Electrochem. Soc.* **2010**, *157*, B1529.
(36) Markovic, N. M.; Grgur, B. N.; Ross, P. N. *J. Phys. Chem. B* **1997**, *101*, 5405.
(37) Zheng, J. P. *Electrochem. Solid-State Lett.* **1999**, *2*, 359.
(38) Bayati, M.; Abad, J. M.; Nichols, R. J.; Schiffrin, D. J. *J. Phys. Chem. C* **2010**, *114*, 18439.
(39) Uyeda, R. *Crystallography of Metal Smoke Particles*; Terra Scientific Publishing Company: Tokyo, Japan, 1987.